Electrochimica Acta 231 (2017) 125–134

Contents lists available at ScienceDirect

Electrochimica Acta

journal homepage: www.elsevier.com/locate/electacta

Electrochemically reduced graphene oxides/nanostructured iron oxides as binder-free electrodes for supercapacitors

Qin Yang[a,*], Ran Bi[a], Kam-chuen Yung[a], Michael Pecht[b]

[a] Department of Industrial and Systems Engineering, The Hong Kong Polytechnic University, Kowloon, Hung Hom, Hong Kong
[b] Center for Advanced Life Cycle Engineering (CALCE), University of Maryland, College Park, MD 20740, USA

ARTICLE INFO

Article history:
Received 13 December 2016
Received in revised form 22 January 2017
Accepted 8 February 2017
Available online 9 February 2017

Keywords:
Electrochemical reduction
Binder-free electrode
Graphene oxides
Iron oxides
Supercapacitors

ABSTRACT

In this work, a facile approach was applied to prepare composites of electrochemically reduced graphene (ecrGO) oxides and iron oxides (FeO_x) as binder-free electrodes for enhancing the electrochemical performance of supercapacitors. The iron oxides were intercalated between the graphene oxides sheets to form sandwich-like composites, such composites were electrochemically reduced in an alkaline solution and directly used as electrodes without any binders. The as-obtained composite (ecrGO/FeO_x) shows a good mechanical strength according to the SEM and Raman results, also exhibits high specific capacitance (C_{sp}) of ~235 F g^{-1} at a scan rate of 10 mV s^{-1} and good cycling stability of 92% retention after 2000 cycles in 1 M NaOH. Although there is a decline of C_{sp} for the ecrGO/FeO_x composite because of the high charge transfer resistance and poor conductivity of the iron oxides, it still possesses a higher C_{sp} than ecrGO when the scan rate increases to 400 mV s^{-1}. The relative high C_{sp} and good stability of ecrGO/iron oxides composites due to the synergistic effect between ecrGO and iron oxides during the electrochemical processes, indicates it can be a promising candidate for supercapacitors.

1. Introduction

The supercapacitor, also called the electrochemical capacitor, is considered to be a promising energy storage device due to its high power density, and fast charging and discharging. The mechanism of a supercapacitor involves a double layer capacitor with physical adsorption-de-adsorption and a pseudocapacitor with fast reversible redox reactions [1]. Carbonaceous materials, such as activated carbon, carbon nanotubes, carbon fibers and graphene, have been are widely investigated for supercapacitors because of their good chemical stability, mechanical strength and conductivity [2–4]. The pseudocapacitors originate from faradic redox reactions of electrode materials like conducting polymers [5,6] or transition metal oxides [7,8].

Graphene has been widely applied in supercapacitors due to the large surface area and high conductivity [9]. However, the experimental measured capacity of graphene is much lower than theoretical value, this is because graphene sheets obtained from the reduction of graphene oxides (GO) easily stack together, resulting in the decrease of surface area and the difficulty for the ions permeating to the surface of graphene [10]. Therefore, graphene-based composites have been developed to facilitate the ion permeability to electrode surface by modifying graphene sheets with carbon materials or metal oxides [11–14].

In terms of metal oxides, iron oxides have been received considerable attention for use in supercapcacitors, due to their low toxicity, natural abundance, environmental friendliness, and chemical and thermodynamical stability [1]. In addition, iron oxides have higher potential for hydrogen evolution in aqueous solutions in contrast with other metal oxides (e.g. nickel oxides or manganese oxides) [15,16]. Also, the pseudocapacitance of the iron oxides can be generated during processes of charge and discharge. These make iron oxide a promising alternative material as an electrode in an aqueous solution for supercapacitors.

In this study, graphene oxide (GO) as graphene precursor and iron oxides as "spacers" were used to obtain the binder-free electrode for supercapacitors, wherein iron oxides can avoid the graphene sheets stacking after being reduced from GO, and also can introduce pseudocapacitance to overall capacitance of graphene based composites. GO can homogenously disperse in water due to the hydrophily of the polar functional groups [17], and these functional groups (such as —COOH and —OH) can make the

* Corresponding author. Tel.: +852 2766 6623.
E-mail address: qin.yang@connect.polyu.hk (Q. Yang).

http://dx.doi.org/10.1016/j.electacta.2017.02.045
0013-4686/

positively charged iron oxides dispersion uniformly adhere to GO sheets. Also the GO can form membrane after drying, so it can serve like a binder to the composites without adding other binders (such as PTFE, PVDF, carbon black).These are the reasons for using GO as graphene precursors.

To achieve better conductivity, GO with poor conductivity [18] are usually reduced to graphene for supercapacitors. Chemical reduction [19], hydrothermal [15,20] or anaerobic thermal [21] reduction are widespread approaches for reducing GO. However these methods are complicated, also special facilities are required. The electrochemical reduction applied in this study is more facile, low-cost and environmentally friendly without the reduction agents, high temperature or vacuum treatment. In addition, the electrochemically reduced GO (ecrGO) can also be directly used as electrodes, dispensing with washing or drying after the reduction process.

In this work, a facile strategy to fabricate a sandwich-like composite of ecrGO/FeO_x as a binder-free electrode for supercapacitors was reported, and the schematic illustration for fabricating electrodes is shown in Fig. 1. The morphology and chemical structure of ecrGO/nanostructured iron oxides composites were investigated using field-emission scanning electronic microscopy (SEM), X-ray diffraction (XRD), Raman, and X-ray Photoelectron spectroscopy (XPS). Also the electrochemical performance of ecrGO/FeO_x composites after electrochemical reduction was measured in alkaline solutions.

2. Experimental

2.1. Synthesis of Fe_2O_3 nanoparticles

1.35 g of $FeCl_3 \cdot 6H_2O$ was dissolved in 60 mL of DI water to obtain a yellow solution. The 5 mL of $NH_3 \cdot H_2O$ was slowly added to the $FeCl_3$ solution, continuously stirring for 20 min, after which a brown precipitates $Fe(OH)_3$ was generated. This brown precipitate was transferred into a 100 ml Teflon-lined stainless steel autoclave, and was subjected to thermal dehydration at 180 °C for 12 h. After cooling to room temperature, the resulting reddish brown paste were washed with distilled water and ethanol for several times, and dried in a vacuum oven at 60 °C. Finally, Fe_2O_3 powder was obtained.

2.2. Preparation of ecrGO/FeO_x electrode

Graphene oxide (5 g L^{-1}, 79% carbon and 20% oxygen) was received from the Graphene-supermarket Inc., USA. 5 g L^{-1} of GO was diluted to 1 g L^{-1} with DI water in a 5-min ultrasonic process. 1 g L^{-1} of Fe_2O_3 suspension was added into the 1 g L^{-1} GO solution with a mass ratio of 1:1, and the mixture was subjected to ultrasonic processing for 30 min, so the Fe_2O_3 was uniformly distributed on the GO sheets. A platinum plate, as a current collector, was covered by the suspension of GO and Fe_2O_3, and dried at 150 °C for 8 min to form the binder-free GO/Fe_2O_3 electrode. The mass loading of the GO/Fe_2O_3 composites on the working electrode was around 3.8 mg cm^{-2}.

Electrochemical reduction of GO/Fe_2O_3 composites with cyclic voltammetry (−1.2 V∼0 V) at a scan rate of 50 mV s^{-1} in 1 M NaOH was carried out using a VersaSTAT potentiostat/galvanostat (Princeton Applied Research, USA) to obtain the composites of electrochemically reduced GO/FeO_x. A three-electrode system with platinum wire as the counter electrode and Ag/AgCl as the reference electrode was applied.

2.3. Materials characterization

The morphology of the iron oxide nanoparticles and GO/Fe_2O_3 composites before and after reduction was characterized by field-emission scanning electronic microscopy (FE-SEM, JEOL JSM-6335F). The phase structure of the iron oxides was detected by an X-ray diffraction (XRD) system (PAN-alytical), ranging from 20° to 70° at a scan rate of 5° min^{-1}. Raman scattering spectra were obtained on a MicroRaman/Photoluminescence spectrometer (Renishaw InVia) with a 633 nm Ar ion laser. X-ray Photoelectron spectroscopy (XPS) on GO/Fe_2O_3 composites before and after electrochemical reduction was conducted using an Axis Ultra DLD X-ray photoelectron spectrometer (Kratos) with an Al K X-ray source. The binding energy was calibrated using C 1s peak at 284.5 eV.

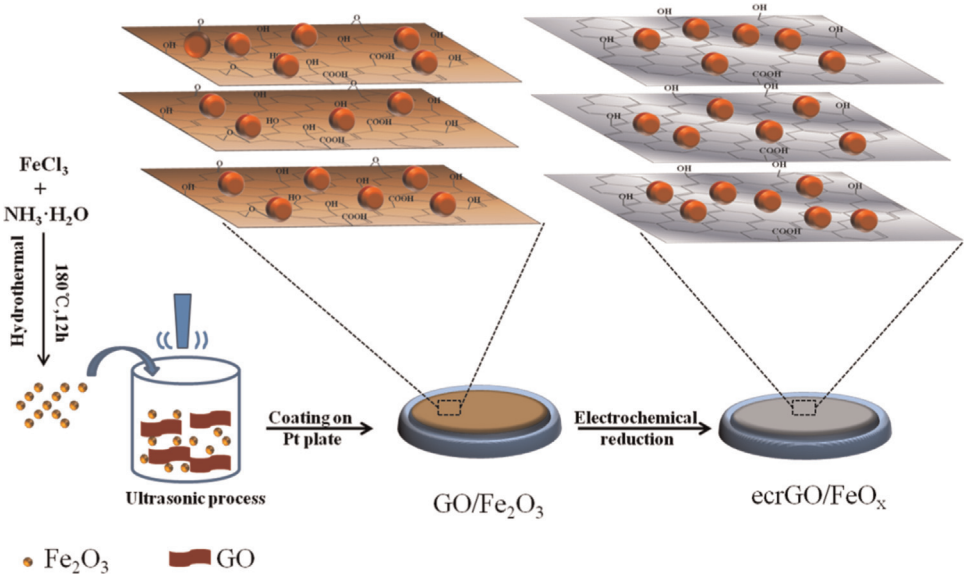

Fig. 1. Schematic illustration for fabricating ecrGO/Fe_2O_3 electrodes.

2.4. Electrochemical measurements

The electrochemical performance of the composites was measured in 1 M NaOH using a VersaSTAT potentiostat/galvanostat (Princeton Applied Research, USA), with platinum wire as the counter electrode and Ag/AgCl as the reference electrode. Cyclic voltammetry (CV), galvanostatic charge-discharge at various current densities and electrochemical impedance spectroscopy (EIS) of the composites were carried out. EIS was applied in a frequency range from 100 kHz to 0.1 Hz with AC amplitude of 5 mV at open-circuit potential.

3. Results and discussion

3.1. Formation of ecrGO/FeO_x electrode by electrochemical reduction

A schematic illustration for fabricating sandwich-like ecrGO/Fe_2O_3 electrodes is shown in Fig. 1. After ultrasonic processing, a uniform suspension of as-received GO sheets and as-synthesized Fe_2O_3 particles was obtained. Here, the GO sheets serve as "scaffolds" for anchoring the Fe_2O_3 particles, and the Fe_2O_3 nanoparticles intercalating between GO sheests can in turn prevent stacking of the graphene sheets when GO is reduced.

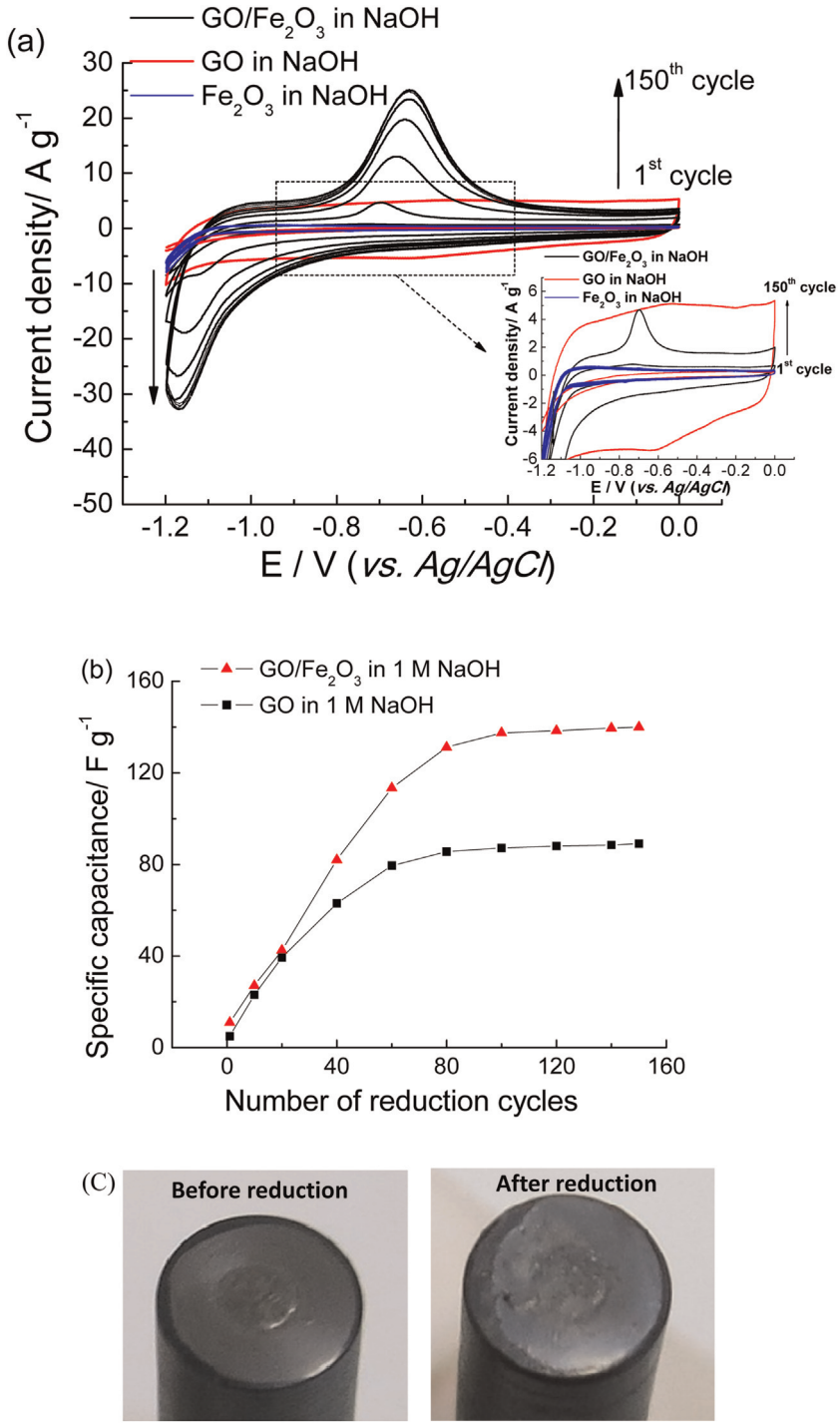

Fig. 2. (a) CV curves of GO and GO/Fe_2O_3 composites in 1 M NaOH from −1.2 V to 0 V (vs.Ag/AgCl) at a scan rate of 50 mV s^{-1}; (b) the specific capacitance of GO and GO/Fe_2O_3 composites in 1 M NaOH as a function of the number of reduction cycles; (c) images of GO/Fe_2O_3 composites before and after electrochemical reduction.

After being coated on the platinum plate, the GO/Fe_2O_3 composites are electrochemically reduced into ecrGO/FeO_x composites and then directly used as electrodes, without any binders.

The electrochemical reduction of GO/Fe_2O_3 composites was carried out using the cyclic voltammetry with a potential range from −1.2 V to 0 V and a scan rate of 50 mV s^{-1}. Fig. 2a shows the CV performance of the GO, Fe_2O_3 and GO/Fe_2O_3 composites during electrochemical reduction in 1 M NaOH at a scan rate of 50 mV s^{-1}. The current densities of GO (the red line in Fig. 2a) and GO/Fe_2O_3 composites (black line in Fig. 2a) increase, along with the number of reduction cycles. As reported in our previous study [22], some functional groups containing oxygen (like C—O—C, —COOH and C—OH) can be reduced by electrochemical reduction, π bonds form. Electrons can transfer via these π bonds of carbon materials, so the GO current increases with increasing numbers of reduction cycles. For the GO/Fe_2O_3 composites, in addition to the increasing current density resulting from the ecrGO formation, a pair of redox peaks appears along with the number of reduction cycles. During negative scanning, reduction peaks appear at −1.15 V due to the electrochemical reduction from Fe^{3+} to Fe^{2+}. During positive scanning, oxidation peaks arise at −0.7 V because of the oxidation from Fe^{2+} to Fe^{3+} [23,24]. The pair of redox peaks become nearly stable after 150 cycles, and is attributed to the redox equilibrium between Fe^{2+} and Fe^{3+}. While the current density of Fe_2O_3 has little increase as shown the insert of Fig. 2a, when compared with GO and GO/Fe_2O_3. This is because iron oxides are almost non-conductive (the large resistance of Fe_2O_3 is provided from EIS spectra in Fig. S1), it is hard for Fe_2O_3 to capture electrons to be reduced. As a result, a better capacitive performance of the GO/Fe_2O_3 composites than the constituents (GO or Fe_2O_3) may be due to the synergistic effect between GO and Fe_2O_3 during the electrochemical reduction. On one hand, GO sheets scattered with Fe_2O_3 particles facilitates electrons or ions transferring to Fe_2O_3, so that redox reaction of Fe_2O_3 can occur more easily. On the other, intercalation of Fe_2O_3 between GO sheets can avoid stack of GO during electrochemical reduction, more charges can be adsorbed on the surface of the composite.

The specific capacitance can be calculated based on the CV curve, using the following equation [25],

$$C_{sp} = \frac{1}{m\nu(V_c - V_a)} \int_{V_a}^{V_c} I(V)dV$$

where C_{sp} is the specific capacitance (F g^{-1}), m is the mass loading of material on the current collector, ν is the potential scan rate (V s^{-1}), (V_c—V_a) is the sweep potential range (V), and $I(V)$ denote the response current (A). Fig. 2b shows the specific capacitance (C_{sp}) of GO and GO/Fe_2O_3 composites in 1 M NaOH with the number of reduction cycles. The C_{sp} of GO increases from the initial C_{sp} of 5 F g^{-1} to 89 F g^{-1}, and becomes stable after 100 reduction cycles. This capacity improvement of GO is mainly from the conductive ecrGO. The specific capacitance of the ecrGO/FeO_x composite becomes stable at 140 F g^{-1}, after undergoing 120 reduction cycles, and the pseudo-capacitance generated from the reversible redox reaction between Fe^{2+} and Fe^{3+} makes a large contribution to the overall capacity of the ecrGO/Fe_2O_x composite. Fig. 2c shows images of GO/Fe_2O_3 composites before (left) and after (right) electrochemical reduction. The color of the GO/Fe_2O_3 composites turns from dark brown before electrochemical reduction to grey luster after electrochemical reduction, and the surface of the electrodes remains flat after the electrochemical reduction. It demonstrates that the ecrGO/Fe_2O_3 composites can be used as binder-free electrodes. Herein, in order to achieve better capacitive performance during electrochemical measurements, the GO/Fe_2O_3 composites applied as binder-free electrodes in this study were subjected to 120 cycles of electrochemical reduction to obtain the ecrGO/FeOx composites

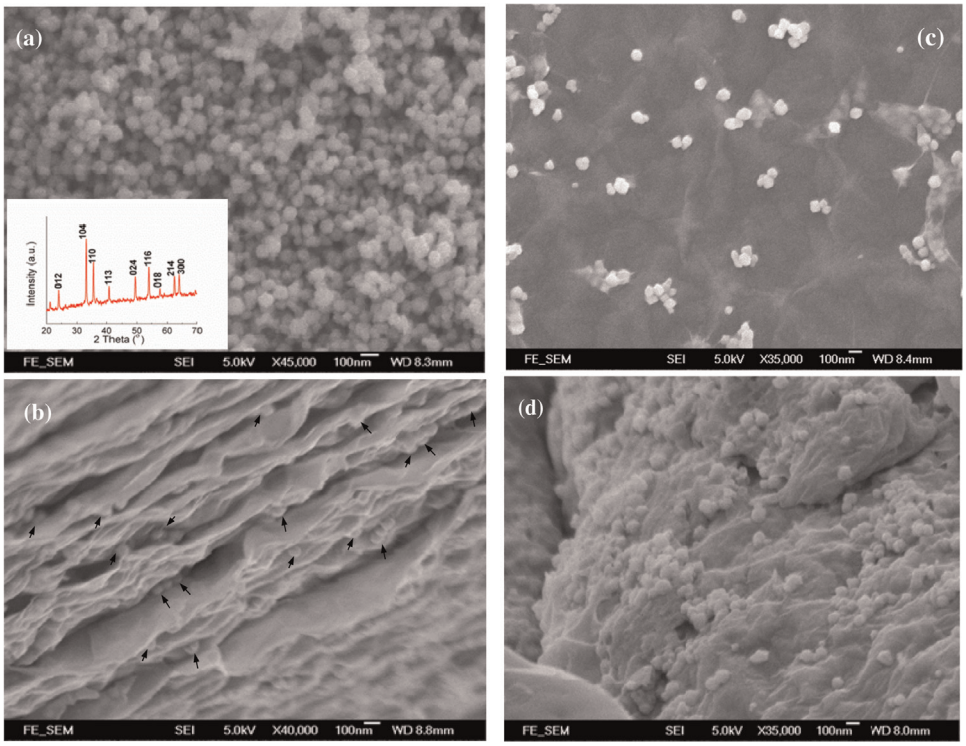

Fig. 3. SEM images of (a) iron oxides with its XRD pattern (inset); (b) cross profile of GO/Fe_2O_3 composites with sandwich-like structure; GO/Fe_2O_3 composites (c) before and (d) after electrochemical reduction.

3.2. Structural characterization of Fe_2O_3, GO/Fe_2O_3 and ecrGO/FeO_x composites

Fig. 3a–c shows the SEM images of the Fe_2O_3 (Fig. 3a), GO/Fe_2O_3 composites (Fig. 3b) and ecrGO/FeO_x composites before and after electrochemical reduction (Fig. 3c and d respectively). The synthesized iron oxides are spherical particles with uniform size around ~70 nm, as shown in Fig. 3a. Their crystal phase should be Fe_2O_3, demonstrated by the XRD results with reflections of (012), (104), (110), (112), (024), (116), (122), (214) and (300) (Fig. 2a, inset) [1,26]. Fig. 3b shows the cross sectional profile of the GO/Fe_2O_3 composites, with Fe_2O_3 nano-particles (indicated by black arrow) inserted between the GO sheets to form sandwich-like structure. Fig. 3c and d show the surface morphology of the GO/Fe_2O_3 composites before and after electrochemical reduction respectively. It can be clearly seen in Fig. 3c that the GO sheets are uniformly dark films with some wrinkles, and Fe_2O_3 particles are isolated on GO sheets. After electrochemical reduction, the iron oxide particles are still uniformly anchored on the ecrGO sheets, as shown in Fig. 3d, it demonstrates that the ecrGO/FeO_x composites exhibit the good mechanical stability.

Fig. 4 shows the Raman spectra of the GO, GO/Fe_2O_3 composites before and after electrochemical reduction. It reveals the characteristic peaks of the D band at ~1340 cm^{-1} corresponding to the vibration of sp3 carbon atoms of the structural defects (such as vacancies, grain boundaries) and disorder, and the G band at ~1580 cm^{-1} indicating in-plane vibration of the sp^2 carbon atoms [11,22,27,28]. The ratio of I_D: I_G for GO is 1.08, and this ratio increases to 1.47 for the GO/Fe_2O_3 composite, meaning a higher disorder degree of the GO/Fe_2O_3 composite than for GO. After being electrochemically reduced, the ratio of I_D: I_G for the ecrGO/FeO_x composite further increases to 1.73. Usually, after reduction of GO, the intensity ratio of I_D:I_G was found to be higher than that of GO without reduction in many reported works [29–31]. The higher I_D: I_G ratio of ecrGO than GO may be related to the higher disorder degree [32,33], defects [34] and smaller average size of sp^2 domain [34–36]. During the electrochemical reduction of GO, the vacant lattice sites are produced due to the removal of oxygenated functional groups in GO. So the defects in reduced GO may not decrease, when compared with GO without reduction [32]. Also, the increased I_D:I_G ratio of reduced GO may be resulted from the decrease in the average size of sp^2 domain [36,37]. Researchers ascribed this observation to the formation of a new graphitic domain with smaller size but greater in numbers [37–40]. These may be the reasons to result in the increased intensity ratio of I_D:I_G for reduced GO. The characteristic peaks at 217 cm^{-1}, 282 cm^{-1}, 405 cm^{-1}, 499 cm^{-1}, and 615 cm^{-1} of both the GO/Fe_2O_3 composites and ecrGO/Fe_2O_3 composites can be observed in Fig. 4, corresponding to the $A_{1g}(1)$, $E_{2g}+E_{3g}$, $A_{1g}(2)$ and E_{5g} modes of Fe_2O_3 [1,41]. It illustrates that iron oxide particles are successfully anchored on the GO sheets, and this Raman spectrum is consistent with the XRD result (insert of Fig. 3a). Also, the Raman patterns of the Fe_2O_3 in the composites before and after electrochemical reduction are almost the same, as black arrows in Fig. 4, indicating the good mechanical stability of the Fe_2O_3 particles before and after electrochemical reduction.

X-ray photoelectron spectroscopy (XPS) is then applied to detect the variation of elemental composition and functional groups. Fig. 5a shows the survey XPS spectra of composites before and after reduction in NaOH, and high resolution XPS spectra of C 1s core-level (Fig. 5b) and Fe 2p core-level (Fig. 5c). The binding energy is calibrated using C 1s peak at 284.6 eV. High peaks around

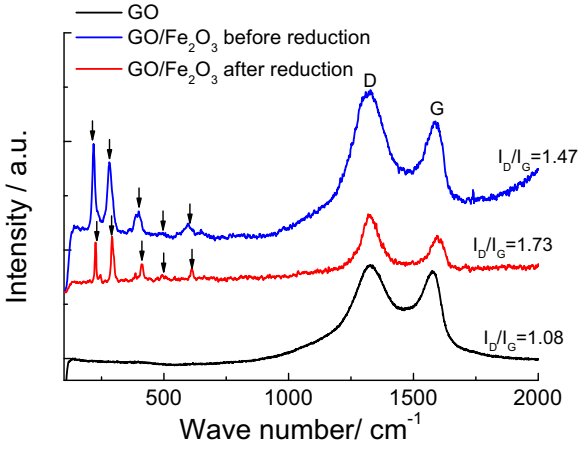

Fig. 4. Raman spectra of GO and GO/Fe_2O_3 composites before and after reduction in 1 M NaOH.

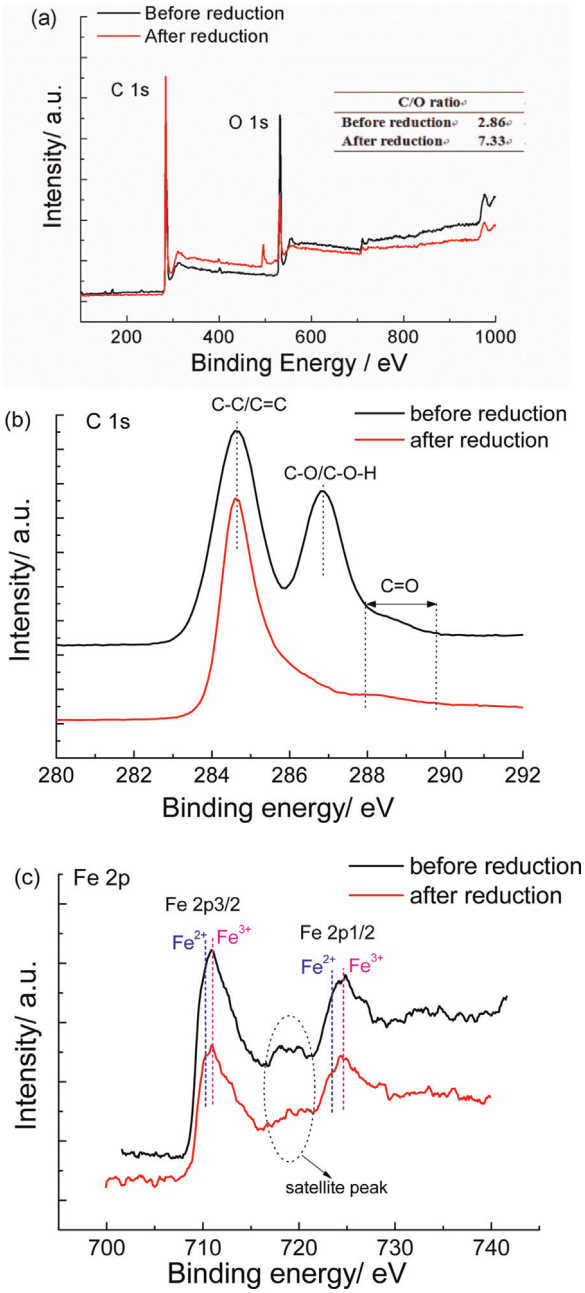

Fig. 5. (a) The survey XPS spectra of composites before and after reduction in NaOH, and high resolution XPS spectra of (b) C 1s core-level and (c) Fe 2p core-level.

285 eV and 533 eV can be clearly observed in Fig. 5a, corresponding to the C 1s and O 1s. The ratio of C/O is 2.86 and 7.33, before and after electrochemical reduction for composites respectively. The higher C/O ratio after electrochemical process indicates GO can be reduced efficiently. Two main peaks in the C1s spectra of the composite before reduction appear at 284.6 eV and 286.8 eV, as shown in Fig. 5b, corresponding to the sp^2-hybridized graphitic carbon (C—C/C=C) in the basal plane and carbon atoms in C—O bonds [42]. The broad peaks in Fig. 5b in the range from 288 eV to 290 eV represent the carbon atoms in carbonyl (C=O/O—C=O) [43]. After reduction in NaOH, the intensity of the peak at 286.8 eV for C 1 s spectra is much lower than the corresponding peak for composites before reduction, meaning that the relative content of functional groups containing C—O bonds decreases a lot after reduction. It demonstrates that the electrochemical reduction of GO mainly results from the reduction of C—O bonds.

Fig. 5c shows the XPS spectra of the Fe 2p core-level for GO/Fe2O3 composites, before and after electrochemical reduction. Binding energies of Fe $2p_{3/2}$ and Fe $2p_{1/2}$ are 711 eV and 724.5 eV respectively for GO/Fe_2O_3 composites before electrochemical reduction, in good agreement with crystalline Fe_2O_3. Also, the characteristic satellite peak of Fe_2O_3 at 719 eV appears before and after electrochemical reduction, further suggesting that the iron oxides before reduction is Fe_2O_3 [44]. Two another peaks at 710.2 eV and 723.5 eV appear for the ecrGO/FeO_x composites, indicating the existence of Fe^{2+} for the composites after electrochemical reduction [45,46]. In the meantime, the satellite peak at 719 eV still appears in the composites after reduction. It may be because Fe^{2+} and Fe^{3+} coexist, and new structures of iron oxides/hydroxides rather than Fe_3O_4 might form during the cyclic voltammetry (CV) cycles between −1.2 V to 0 V. The reduction from Fe^{3+} to Fe^{2+} may result from cation intercalation [23] (such as H^+ or Na^+ in electrolyte).

3.3. Electrochemical performance of ecrGO/FeO_x composites as binder-free electrodes

To evaluate the capacitive performance of ecrGO/FeO_x composites (working potential ranging from −1.2 V to 0 V *vs.* Ag/AgCl), cyclic voltammetry (CV), EIS and galvanostatic charge/discharge are applied in a three-electrode system. The rate-dependent CV curves of the ecrGO and ecrGO/FeO_x composites were measured in 1 M NaOH with the working potential window between −1.2 V and 0 V. Fig. 6a and b show the CV curves of the ecrGO and ecrGO/Fe_2O_3 composites for different scan rates. The CV curves of ecrGO (Fig. 6b) under scan rates ranging from 10 mV s^{-1} to 400 mV s^{-1} display a quasi-rectangular shape with little distortion, indicating that ecrGO behaves almost as a ideal double-layer capacitor. The ecrGO/FeO_x composite can basically exhibit a stable capacitive behavior when the scan rates increase, while the slight distortion of its CV curves when the scan rate increases to 400 mV s^{-1} (Fig. 6a), is mainly attributed to the poor conductivity of Fe_2O_3. Hence the loss of capacity for composites under higher scan rates may resulte from the weaker conductivity of the composite than the ecrGO. Besides, a pair of redox peaks of the ecrGO/FeOx composites appears around −0.7 V and −1.12 V when scan rate is 10 mV s^{-1}, with the anodic peaks shifting positively and the cathodic peaks shifting negatively with the increasing scanning rates, as shown in Fig. 6a. This shift may be caused by the electrochemical polarization of the reversible reaction between Fe^{2+}/Fe^{3+}. So the working potential window for galvanostatic tests of charge and discharge ranges from −1.12 V to 0 V to avoid the hydrogen emission during charge and discharge. When the scan rates become faster, the electrochemical reaction is unable to keep the pace with the electron transfer due to the high charge transfer resistance (R_{ct}), resulting in the anodic or cathodic peak being more positive or negative. This also may be the reason why the CV curves of the composites are slightly distorted under higher scan rates. The large R_{ct} of the ecrGO/FeO_x composites is further illustrated by the EIS results.

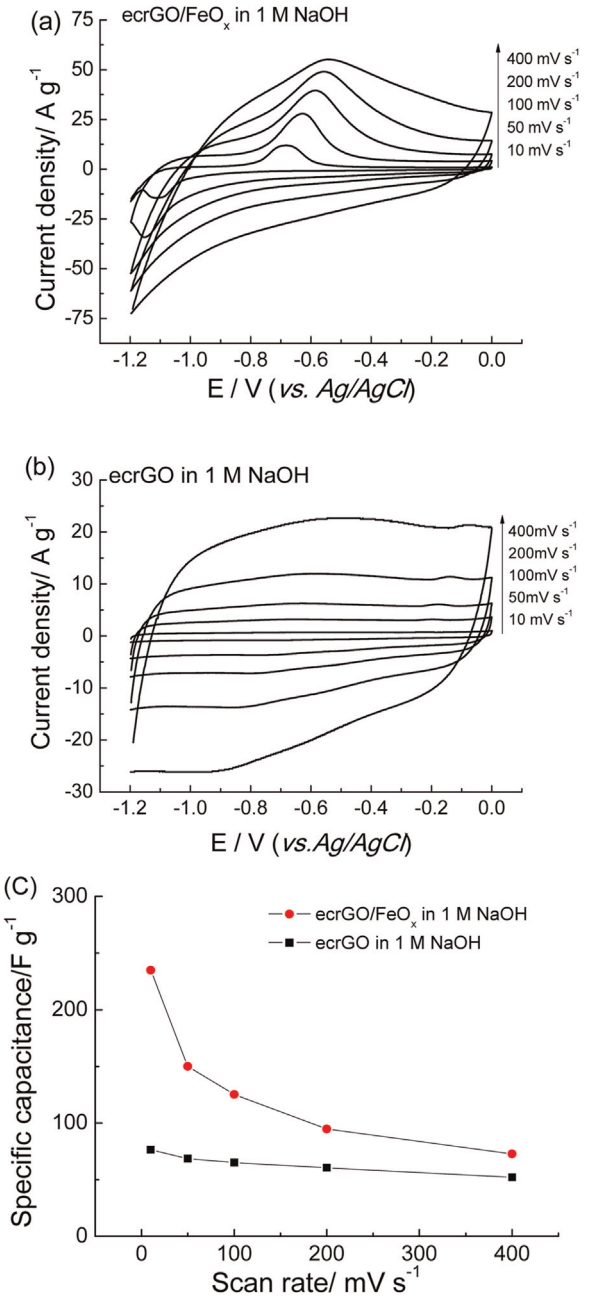

Fig. 6. CV curves of (a) ecrGO/FeOx electrode and (b) ecrGO in 1 M NaOH at various scan rates of 10 mV s^{-1}, 50 mV s^{-1}, 100 mV s^{-1}, 200 mV s^{-1}, 400 mV s^{-1}; (c) the specific capacitance of ecrGO and ecrGO/FeOx electrode as a function of different scan rates.

Additionally, Fig. 6c shows the specific capacitance of the ecrGO/FeO_x composites and ecrGO, under various scan rates. The specific capacitance (C_{sp}) of the ecrGO/FeOx composites decreases from ~235 F g^{-1} to 74 F g^{-1} when the scan rate increases from 10 mV s^{-1} to 400 mV s^{-1}, while there is a very small reduction for the C_{sp} of ecrGO (from ~76 F g^{-1} to ~54 F g^{-1}). Although the ecrGO/FeO_x composites show higher specific capacitance (C_{sp}) than ecrGO under different scan rates, the C_{sp} of ecrGO/FeO_x composites drops faster than ecrGO with increasing scan rates. The distortion of the CV curves and the capacitive loss at high scan rates of the ecrGO/

FeO_x composites, when compared with ecrGO, may be caused by the lower conductivity and high R_{ct} of iron oxides. Therefore, although the specific capacitance of composites can be enhanced by introducing iron oxides into ecrGO, it does not mean that iron oxides in composites always benefit the capacitive performance, especially at high rates of charge and discharge.

The energy densities and power densities calculated are shown in Fig. 7, using the following equations [14]

$$\text{Energy density} = \frac{1}{2 \times 3.6} \times C_{sp} \times \Delta U^2$$

$$\text{Power density} = \frac{Energy\ density}{t_{discharge}}$$

where C_{sp} is the specific capacitance of electrodes ($F\,g^{-1}$), ΔU is the potential window (V), the unit for energy density is $Wh\,kg^{-1}$. $t_{discharge}$ is the time of discharge (hour), and the unit for power density is $W\,kg^{-1}$. The energy densities of ecrGO/FeO_x composites are 47, 30, 25, 19, 15 $Wh\,kg^{-1}$ at power densities 1.41, 4.5, 7.5, 11.4, and 18 $kW\,kg^{-1}$, respectively. The energy densities of ecrGO/FeO_x composite are higher than that of ecrGO at the same power densities.

To further compare and understand the electrochemical kinetics of ecrGO/FeO_x composites and ecrGO for supercapacitors, electrochemical impedance spectroscopy (EIS) measurements were conducted from 100 kHz to 0.1 Hz, with an AC amplitude of 5 mV at open circuit potential. Fig. 8a shows typical Nyquist plots of the ecrGO/FeO_x composites and ecrGO, including semi-circles in the high-frequency range (Fig. 8a) and straight lines in the low-frequency range (the insert in Fig. 8a). The semi-circle in the high-frequency range corresponds to the charge transfer resistance relating to the faradic process [47]. A portion of the straight line with slope nearly 45° at the mid-frequency, as shown the insert in Fig. 8a (the magnification of Nyquist plot in the high-frequency region and the mid-frequency region), indicates the electrochemical behavior is controlled by the diffusion process [8]. In the low-frequency range, the more vertical lines, representing a rapid ion diffusion in the electrolyte and ion adsorption onto the surface of materials, suggests a more ideal capacitive performance of the electrodes [48]. The larger semi-circle of ecrGO/FeO_x composites compared to that of ecrGO means a higher R_{ct}, and can be attributed to the faradic process between Fe^{2+} and Fe^{3+}. The higher R_{ct} of ecrGO/FeO_x composites than ecrGO also can provide an explanation that the CV curve is more likely to be distorted (Fig. 6a). The more vertical straight line in the low-frequency region of ecrGO compared to the ecrGO/FeO_x composite indicates

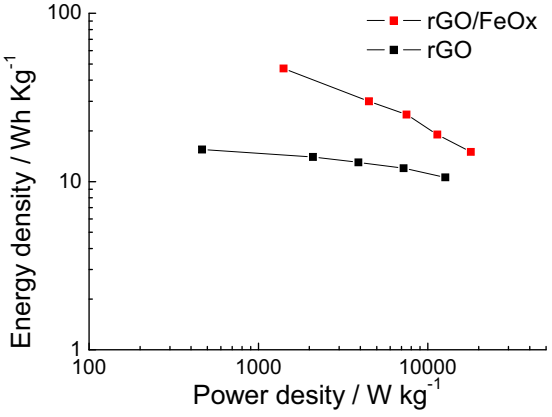

Fig. 7. Regone plot of ecrGO and ecrGO/FeO_x composite.

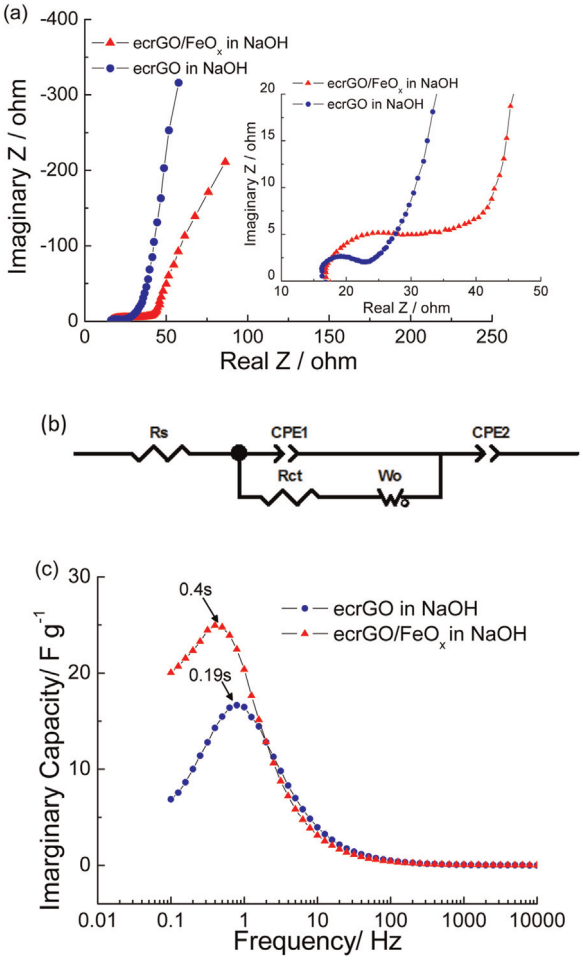

Fig. 8. (a) EIS spectra of ecrGO/FeO_x composites and ecrGO with frequencies ranged from 100 kHz to 0.1 Hz with amplitude of 5 mV at OCV; (b) the equivalent circuit for fitting EIS spectrum; (c) imaginary part of capacity (C") as a functional of frequency.

the more ideal capacitive performance of ecrGO. This is due to the less faradic effect generated from Fe^{2+}/Fe^{3+} for ecrGO, thus ecrGO more likely acts as a double-layer capacitor than ecrGO/FeO_x.

An equivalent circuit model for fitting EIS data is shown in Fig. 8b. The high-frequency intercept with real axis and semi-circle correspond to the electrolyte resistance (R_s) and the charge transfer resistance (R_{ct}), respectively. The portion of the straight line with slope nearly 45° at the mid-frequency represents the Warburg resistance (W_o) of ionic diffusion from electrolyte to the surface of electrode, in series with R_{ct}. The Warburg element is selected due to the frequency dependence of porous materials and counter ion diffusion to electrode surface during faradic process [49]. Constant phase elements (CPE_1), in parallel with R_{ct} and W_o, is used to model the semicircle in high frequency. And CPE_2 is applied to describe the nearly vertical line in low frequency [14]. From the model, the R_{ct} values for the ecrGO and the ecrGO/FeO_x composite are 6.6 Ω and 19.5 Ω, respectively. The higher R_{ct} of the ecrGO/FeO_x composite than that of the ecrGO mainly results from faradic process between Fe^{2+} and Fe^{3+}. The Warburg resistance of the ecrGO/FeO_x composite is 26 Ω and Warburg resistance of the ecrGO is 28.8 Ω. The smaller Warburg resistance of the ecrGO/FeO_x composite means the more effective diffusion process from electrolyte to electrode surface, when compared with ecrGO. The better ionic diffusion process for the ecrGO/FeO_x composite may be attributed to intercalation of iron oxide particles between ecrGO sheets, facilitating ionic diffusion to the surface of ecrGO/FeO_x composites.

Fig. 8c represents the imaginary part of the capacitance (C") as a functional of frequency. The imaginary part of capacitance corresponds to the energy dissipation of the capacitor and is a characteristic of an irreversible process, which can result in the hysteresis of the electrochemical process [50,51]. The C" goes through the maximum value at a frequency known as the relaxation frequency f_R, so the characteristic time constant τ_0 can be determined according to the equation ($\tau_0 = (2\pi f_R)^{-1}$) [51]. τ_0 is the minimum time required to discharge all the energy with an efficiency more than 50% of its maximum value [52,53]. The constant times of 0.19 s and 0.4 s are obtained for ecrGO and ecrGO/FeO_x composites respectively, meaning a faster discharging time of the ecrGO than that of the ecrGO/Fe_2O_3 composites. It may be due to the less faradic effect in ecrGO than the ecrGO/FeO_x composite.

The galvanostatic charge and discharge of ecrGO/FeO_x composites and ecrGO in long-term cycle was carried out under various constant current densities (1 A g^{-1}, 2 A g^{-1}, 4 A g^{-1}) to detect the stability. The specific capacity of electrodes can be obtained at different constant current densities according to the equation below:

$$C_{sp} = \frac{I\Delta t}{m(V_2 - V_1)}$$

Where I/m (A g^{-1}) is the constant current density for charge and discharge, Δt (s) is the time duration for discharging, V_1 (V) and V_2 (V) are the initial and final potentials for discharge respectively. All the charge/discharge curves under different current densities have a triangular shape with little distortion, as shown in Fig. 9 inserts, suggesting the ecrGO/FeO_x composites and ecrGO exhibit capacitive behavior. For charge and discharge curves of ecrGO/FeO_x composites shown in Fig. 9a, the platforms of charging and discharging can be observed at −1.1 V and −0.7 V at a current density of 1 A g^{-1}, correspondingly. This charging/discharge platform is contributed from the reversible reaction between Fe^{2+} and Fe^{3+}, in agreement with the CV results in Fig. 2a. When the current density increases to 2 A g^{-1}, the duration of the charging/discharging platform shorten. This platform is barely observed when the current density further increases to 4 A g^{-1}. It can be attributed to the more severe polarization resulted from the internal resistance and charge transfer resistance when higher current passed through the electrodes. For charge and discharge curves of ecrGO shown in Fig. 9b insert, platforms are hardly observed, attributing to the little redox reaction on ecrGO.

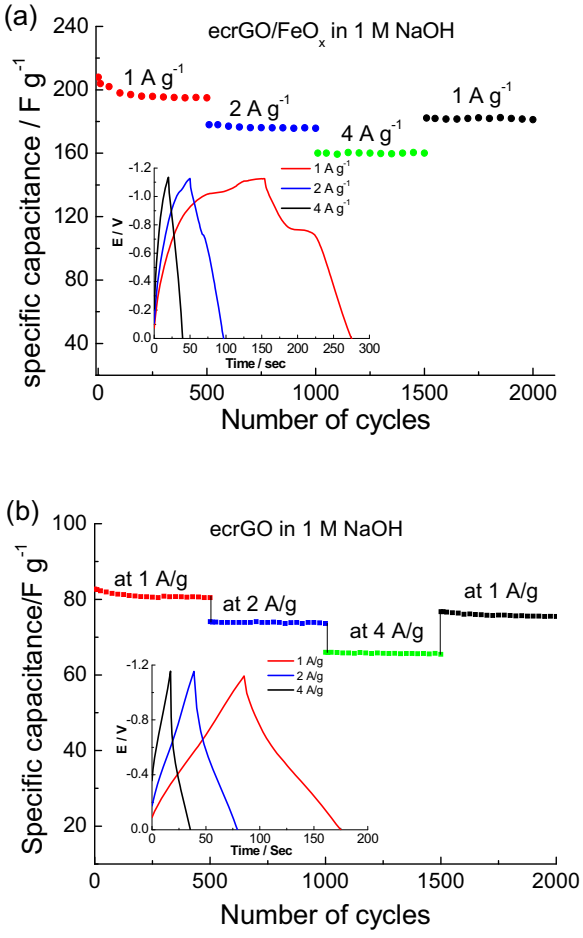

Fig. 9. cycling performance of (a) ecrGO/FeO_x composites and (b) ecrGO for 2000 cycles, insert shows the galvanostatic charge and discharge curves at various current densities (1 A g^{-1}, 2 A g^{-1}, 4 A g^{-1}).

The specific capacity of ecrGO/FeO_x composites and ecrGO for 2000 cycles of charge and discharge were measured, as shown in Fig. 9. For ecrGO/FeO_x composite shown in Fig. 9a, a C_{sp} value of 195 F g^{-1} can be obtained at a current density of 1 A g^{-1} after 500 cycles, and its C_{sp} of 176 F g^{-1} (~10% drop) at 2 A $g^{-1}$and 160 F g^{-1} (~18% drop) at 4 A g^{-1} are obtained, when cycle number goes to the 1000 and 1500, respectively. The measured C_{sp} is 181 F g^{-1} at the 2000th cycle, when the current density returns to 1 A g^{-1}, and a retention of 92% can be obtained after 2000 cycles of charge and discharge, indicating good electrochemical stability for the ecrGO/FeO_x composite. The small decrease of C_{sp} for the composites may be due to the fading of FeO_x during the long life cycle of charge and discharge. As shown in Fig. 9b, the calculated C_{sp} of ecrGO is 80 F g^{-1}, 73 F g^{-1} and 66 F g^{-1} under current density of 1 A g^{-1}, 2 A g^{-1}, and 4 A g^{-1}, respectively. The C_{sp} value of 75 F g^{-1} can be obtained when current density turns back to 1 A g^{-1}. The retention for ecrGO after 2000 cycles of charge and discharge is 93.7%, slightly higher than that of ecrGO/FeO_x composites.

Table 1 shows the comparison of the specific capacitance of rGO/iron oxides among the reported works and this work. The capacitive performance of rGO/iron oxides composites varies maybe because of the different structures of iron oxides, the treatment of reduced GO, different current collectors and various testing methods. The specific capacitance of ecrGO/iron oxides composites in this work shows the relative high value, although it is not the best one among those reported works. Here, this work mainly presents a facile strategy for fabricating reduced GO/iron oxides composites, as binder-free electrodes for supercapacitors, via electrochemical process. Also the study illustrates the synergistic effect between ecrGO and iron oxides during the electrochemical process. The relative high C_{sp} of ecrGO/iron oxides composites in potential range from −1.2 V to 0 V indicates it can be a promising candidate as an anode when fabricating an asymmetric supercapacitor.

4. Conclusions

Sandwich-like composites of electrochemical reduced GO and iron oxides with relative high specific capacitance and retention were developed for supercapacitors. A facile electrochemical reduction approach was applied to reduce GO to ecrGO in an alkaline solution, after electrochemical reduction the ecrGO/FeO_x composite can be directly used as electrodes without any binders. This sandwich-like ecrGO/FeO_x composite exhibits a high C_{sp} (195 F g^{-1} at 1 A g^{-1}, 235 F g^{-1} at a scan rate of 10 mV s^{-1}) and good cycling stability (92% retention after 2000 charging/discharging cycles) because of the synergistic effect between ecrGO and iron oxides in ecrGO/FeO_x composites. The ecrGO can act as a framework for anchoring the iron oxides, which in turn can introduce pseudocapacitance to the composites and hinder the

Table 1
A comparison of C_{sp} of rGO/iron oxides for supercapacitors among reported works and this work.

Sample	Current density or scan rate	Specific capacitance ($F\,g^{-1}$)	Reference
ecrGO/FeO_x in 1 M NaOH	10 mV s^{-1}	235	This work
Fe_2O_3/rGO in 1 M Na_2SO_4	10 mV s^{-1}	180	[54]
Fe_2O_3/N-rGO in 1 M KOH	1 A g^{-1}	550	[11]
Fe_2O_3-GO in 2 M KOH	1 A g^{-1}	150	[55]
rGO/Fe_3O_4 in 0.5 M Na_2SO_4	1 A g^{-1}	236	[14]
α-Fe_2O_3/rGO in 0.1 K_2SO_4	20 mV s^{-1}	113	[15]
Fe_3O_4/rGO in 1 M Na_2SO_3	1 A g^{-1}	262	[56]

stacking of the ecrGO sheets. Also, the composites have a good mechanical strength, as indicated in the SEM and Raman results. The ecrGO/FeO_x composite possesses much higher C_{sp} than ecrGO due to the pseudocapacitance of the iron oxides, although the C_{sp} of the ecrGO/FeO_x composites decrease with the increasing discharge rates because of the high R_{ct} and poor conductivity of the iron oxides. Hence, iron oxides in composites do not always benefit the capacitive performance, especially at high rates of charge and discharge. The optimal combination of ecrGO and iron oxides needs to be studied further. The ecrGO/FeO_x composite reported here is still a good candidate for supercapacitors. This composite as a binder-free anode for an asymmetric supercapacitor will be fabricated and investigated in our following research.

Acknowledgement

The work described in this paper was partially supported by the Research Committee of The Hong Kong Polytechnic University under project No. RTAP and the National Natural Science Foundation of China (Project No. 61473242)

Appendix A. Supplementary data

Supplementary data associated with this article can be found, in the online version, at http://dx.doi.org/10.1016/j.electacta.2017.02.045.

References

[1] H. Zhang, Q. Gao, K. Yang, Y. Tan, W. Tian, L. Zhu, Z. Li, C. Yang, Solvothermally induced [small alpha]-Fe2O3/graphene nanocomposites with ultrahigh capacitance and excellent rate capability for supercapacitors, Journal of Materials Chemistry A 3 (2015) 22005–22011.
[2] C. Portet, P.L. Taberna, P. Simon, E. Flahaut, C. Laberty-Robert, High power density electrodes for Carbon supercapacitor applications, Electrochimica Acta 50 (2005) 4174–4181.
[3] L.L. Zhang, X.S. Zhao, Carbon-based materials as supercapacitor electrodes, Chemical Society Reviews 38 (2009) 2520–2531.
[4] G. Wang, L. Zhang, J. Zhang, A review of electrode materials for electrochemical supercapacitors, Chemical Society Reviews 41 (2012) 797–828.
[5] D.S. Dhawale, R.R. Salunkhe, V.S. Jamadade, D.P. Dubal, S.M. Pawar, C.D. Lokhande, Hydrophilic polyaniline nanofibrous architecture using electrosynthesis method for supercapacitor application, Current Applied Physics 10 (2010) 904–909.
[6] L.-Z. Fan, J. Maier, High-performance polypyrrole electrode materials for redox supercapacitors, Electrochemistry Communications 8 (2006) 937–940.
[7] R.N. Reddy, R.G. Reddy, Sol–gel MnO2 as an electrode material for electrochemical capacitors, Journal of Power Sources 124 (2003) 330–337.
[8] J. Xu, L. Gao, J. Cao, W. Wang, Z. Chen, Preparation and electrochemical capacitance of cobalt oxide (Co3O4) nanotubes as supercapacitor material, Electrochimica Acta 56 (2010) 732–736.
[9] Q. Cheng, J. Tang, J. Ma, H. Zhang, N. Shinya, L.-C. Qin, Graphene and carbon nanotube composite electrodes for supercapacitors with ultra-high energy density, Physical Chemistry Chemical Physics 13 (2011) 17615–17624.
[10] N. Jung, S. Kwon, D. Lee, D.-M. Yoon, Y.M. Park, A. Benayad, J.-Y. Choi, J.S. Park, Synthesis of Chemically Bonded Graphene/Carbon Nanotube Composites and their Application in Large Volumetric Capacitance Supercapacitors, Advanced Materials 25 (2013) 6854–6858.
[11] Z. Ma, X. Huang, S. Dou, J. Wu, S. Wang, One-Pot Synthesis of Fe2O3 Nanoparticles on Nitrogen-Doped Graphene as Advanced Supercapacitor Electrode Materials, The Journal of Physical Chemistry C 118 (2014) 17231–17239.
[12] Y. Gao, D. Wu, T. Wang, D. Jia, W. Xia, Y. Lv, Y. Cao, Y. Tan, P. Liu, One-step solvothermal synthesis of quasi-hexagonal Fe2O3 nanoplates/graphene composite as high performance electrode material for supercapacitor, Electrochimica Acta 191 (2016) 275–283.
[13] S. Yang, X. Song, P. Zhang, J. Sun, L. Gao, Self-Assembled α-Fe2O3 Mesocrystals/Graphene Nanohybrid for Enhanced Electrochemical Capacitors, Small 10 (2014) 2270–2279.
[14] S. Ghasemi, F. Ahmadi, Effect of surfactant on the electrochemical performance of graphene/iron oxide electrode for supercapacitor, Journal of Power Sources 289 (2015) 129–137.
[15] K.K. Lee, S. Deng, H.M. Fan, S. Mhaisalkar, H.R. Tan, E.S. Tok, K.P. Loh, W.S. Chin, C.H. Sow, [small alpha]-Fe2O3 nanotubes-reduced graphene oxide composites as synergistic electrochemical capacitor materials, Nanoscale 4 (2012) 2958–2961.
[16] P. Simon, Y. Gogotsi, Materials for electrochemical capacitors, Nat Mater 7 (2008) 845–854.
[17] S. Park, R.S. Ruoff, Chemical methods for the production of graphenes, Nat Nano 4 (2009) 217–224.
[18] S. Pei, H.-M. Cheng, The reduction of graphene oxide, Carbon 50 (2012) 3210–3228.
[19] C.K. Chua, M. Pumera, Chemical reduction of graphene oxide: a synthetic chemistry viewpoint, Chemical Society Reviews 43 (2014) 291–312.
[20] D. Wang, Y. Li, Q. Wang, T. Wang, Nanostructured Fe2O3–graphene composite as a novel electrode material for supercapacitors, Journal of Solid State Electrochemistry 16 (2011) 2095–2102.
[21] C. Long, T. Wei, J. Yan, L. Jiang, Z. Fan, Supercapacitors Based on Graphene-Supported Iron Nanosheets as Negative Electrode Materials, ACS Nano 7 (2013) 11325–11332.
[22] Q. Yang, S.-K. Pang, K.-C. Yung, Electrochemically reduced graphene oxide/carbon nanotubes composites as binder-free supercapacitor electrodes, Journal of Power Sources 311 (2016) 144–152.
[23] Q. Qu, S. Yang, X. Feng, 2D Sandwich-like Sheets of Iron Oxide Grown on Graphene as High Energy Anode Material for Supercapacitors, Advanced Materials 23 (2011) 5574–5580.
[24] S. Virtanen, P. Schmuki, M. Büchler, H.S. Isaacs, Electrochemical Behavior of Fe in Phosphate Solutions Studied by In Situ X-Ray Absorption Near Edge Structure, Journal of The Electrochemical Society 146 (1999) 4087–4094.
[25] Q. Yang, S.-K. Pang, K.-C. Yung, Study of PEDOT–PSS in carbon nanotube/conducting polymer composites as supercapacitor electrodes in aqueous solution, Journal of Electroanalytical Chemistry 728 (2014) 140–147.
[26] D. Maiti, V. Aravindan, S. Madhavi, P. Sujatha Devi, Electrochemical performance of hematite nanoparticles derived from spherical maghemite and elongated goethite particles, Journal of Power Sources 276 (2015) 291–298.
[27] K. Ai, Y. Liu, L. Lu, X. Cheng, L. Huo, A novel strategy for making soluble reduced graphene oxide sheets cheaply by adopting an endogenous reducing agent, Journal of Materials Chemistry 21 (2011) 3365–3370.
[28] N.A. Kumar, H.-J. Choi, Y.R. Shin, D.W. Chang, L. Dai, J.-B. Baek, Polyaniline-Grafted Reduced Graphene Oxide for Efficient Electrochemical Supercapacitors, ACS Nano 6 (2012) 1715–1723.
[29] G.T.S. How, A. Pandikumar, H.N. Ming, L.H. Ngee, Highly exposed {001} facets of titanium dioxide modified with reduced graphene oxide for dopamine sensing, Sci. Rep. 4 (2014).
[30] C. Chen, M. Long, M. Xia, C. Zhang, W. Cai, Reduction of graphene oxide by an in-situ photoelectrochemical method in a dye-sensitized solar cell assembly, Nanoscale Research Letter 7 (2012) 101.
[31] M. Mishra, A.P. Singh, B.P. Singh, S.K. Dhawan, Performance of a nanoarchitectured tin oxide@reduced graphene oxide composite as a shield against electromagnetic polluting radiation, RSC Advances 4 (2014) 25904–25911.
[32] C. Gómez-Navarro, R.T. Weitz, A.M. Bittner, M. Scolari, A. Mews, M. Burghard, K. Kern, Electronic Transport Properties of Individual Chemically Reduced Graphene Oxide Sheets, Nano Letters 7 (2007) 3499–3503.
[33] X.-Y. Peng, X.-X. Liu, D. Diamond, K.T. Lau, Synthesis of electrochemically-reduced graphene oxide film with controllable size and thickness and its use in supercapacitor, Carbon 49 (2011) 3488–3496.
[34] B. Zhao, P. Liu, Y. Jiang, D. Pan, H. Tao, J. Song, T. Fang, W. Xu, Supercapacitor performances of thermally reduced graphene oxide, Journal of Power Sources 198 (2012) 423–427.

[35] S.Y. Toh, K.S. Loh, S.K. Kamarudin, W.R.W. Daud, Graphene production via electrochemical reduction of graphene oxide: Synthesis and characterisation, Chemical Engineering Journal 251 (2014) 422–434.
[36] Y. Jiang, Y. Lu, F. Li, T. Wu, L. Niu, W. Chen, Facile electrochemical codeposition of clean graphene–Pd nanocomposite as an anode catalyst for formic acid electrooxidation, Electrochemistry Communications 19 (2012) 21–24.
[37] Z. Ji, X. Shen, M. Li, H. Zhou, G. Zhu, K. Chen, Synthesis of reduced graphene oxide/CeO 2 nanocomposites and their photocatalytic properties, Nanotechnology 24 (2013) 115603.
[38] Y.-G. Zhou, J.-J. Chen, F.-B. Wang, Z.-H. Sheng, X.-H. Xia, A facile approach to the synthesis of highly electroactive Pt nanoparticles on graphene as an anode catalyst for direct methanol fuel cells, Chemical Communications 46 (2010) 5951–5953.
[39] H.-L. Guo, X.-F. Wang, Q.-Y. Qian, F.-B. Wang, X.-H. Xia, A green approach to the synthesis of graphene nanosheets, ACS Nano 3 (2009) 2653–2659.
[40] S. Stankovich, D.A. Dikin, R.D. Piner, K.A. Kohlhaas, A. Kleinhammes, Y. Jia, Y. Wu, S.T. Nguyen, R.S. Ruoff, Synthesis of graphene-based nanosheets via chemical reduction of exfoliated graphite oxide, Carbon 45 (2007) 1558–1565.
[41] D.L.A. de Faria, S. Venâncio Silva, M.T. de Oliveira, Raman microspectroscopy of some iron oxides and oxyhydroxides, Journal of Raman Spectroscopy 28 (1997) 873–878.
[42] N. Han, T. Viet Cuong, M. Han, B. Deul Ryu, S. Chandramohan, J. Bae Park, J. Hye Kang, Y.-J. Park, K. Bok Ko, H. Yun Kim, H. Kyu Kim, J. Hyoung Ryu, Y.S. Katharria, C.-J. Choi, C.-H. Hong, Improved heat dissipation in gallium nitride light-emitting diodes with embedded graphene oxide pattern, Nat Commun 4 (2013) 1452.
[43] Q. Yang, S.-K. Pang, K.-C. Yung, Dynamic high potential treatment with dilute acids for lifting the capacitive performance of carbon nanotube/conducting polymer electrodes, Journal of Electroanalytical Chemistry 758 (2015) 125–134.
[44] X. Zhang, Y. Niu, X. Meng, Y. Li, J. Zhao, Structural evolution and characteristics of the phase transformations between [small alpha]-Fe2O3, Fe3O4 and [gamma]-Fe2O3 nanoparticles under reducing and oxidizing atmospheres, CrystEngComm 15 (2013) 8166–8172.
[45] M.E. Im, D. Pham-Cong, J.Y. Kim, H.S. Choi, J.H. Kim, J.P. Kim, J. Kim, S.Y. Jeong, C. R. Cho, Enhanced electrochemical performance of template-free carbon-coated iron(II, III) oxide hollow nanofibers as anode material for lithium-ion batteries, Journal of Power Sources 284 (2015) 392–399.
[46] A. Koehl, D. Kajewski, J. Kubacki, C. Lenser, R. Dittmann, P. Meuffels, K. Szot, R. Waser, J. Szade, Detection of Fe2+ valence states in Fe doped SrTiO3 epitaxial thin films grown by pulsed laser deposition, Physical Chemistry Chemical Physics 15 (2013) 8311–8317.
[47] P. Zhao, W. Li, G. Wang, B. Yu, X. Li, J. Bai, Z. Ren, Facile hydrothermal fabrication of nitrogen-doped graphene/Fe2O3 composites as high performance electrode materials for supercapacitor, Journal of Alloys and Compounds 604 (2014) 87–93.
[48] A. Ramadoss, S.J. Kim, Improved activity of a graphene–TiO2 hybrid electrode in an electrochemical supercapacitor, Carbon 63 (2013) 434–445.
[49] D. Antiohos, K. Pingmuang, M.S. Romano, S. Beirne, T. Romeo, P. Aitchison, A. Minett, G. Wallace, S. Phanichphant, J. Chen, Manganosite–microwave exfoliated graphene oxide composites for asymmetric supercapacitor device applications, Electrochimica Acta 101 (2013) 99–108.
[50] H. Kurig, A. Jänes, E. Lust, Electrochemical Characteristics of Carbide-Derived Carbonl1-Ethyl-3-methylimidazolium Tetrafluoroborate Supercapacitor Cells, Journal of The Electrochemical Society 157 (2010) A272–A279.
[51] T. Thomberg, A. Jänes, E. Lust, Energy and power performance of electrochemical double-layer capacitors based on molybdenum carbide derived carbon, Electrochimica Acta 55 (2010) 3138–3143.
[52] K. Sheng, Y. Sun, C. Li, W. Yuan, G. Shi, Ultrahigh-rate supercapacitors based on eletrochemically reduced graphene oxide for ac line-filtering, Scientific Reports 2 (2012) 247.
[53] P.L. Taberna, P. Simon, J.F. Fauvarque, Electrochemical Characteristics and Impedance Spectroscopy Studies of Carbon-Carbon Supercapacitors, Journal of The Electrochemical Society 150 (2003) A292–A300.
[54] Z. Wang, C. Ma, H. Wang, Z. Liu, Z. Hao, Facilely synthesized Fe2O3–graphene nanocomposite as novel electrode materials for supercapacitors with high performance, Journal of Alloys and Compounds 552 (2013) 486–491.
[55] D. Wang, Y. Li, Q. Wang, T. Wang, Nanostructured Fe2O3–graphene composite as a novel electrode material for supercapacitors, Journal of Solid State Electrochemistry 16 (2012) 2095–2102.
[56] J.P. Cheng, Q.L. Shou, J.S. Wu, F. Liu, V.P. Dravid, X.B. Zhang, Influence of component content on the capacitance of magnetite/reduced graphene oxide composite, Journal of Electroanalytical Chemistry 698 (2013) 1–8.